

Published in final edited form as:

J Org Chem. 2013 March 1; 78(5): 1753–1759. doi:10.1021/jo3011792.

Control of Regioselectivity and Stereoselectivity in (4+3) Cycloadditions of Chiral Oxyallyls with Unsymmetrically Disubstituted Furans

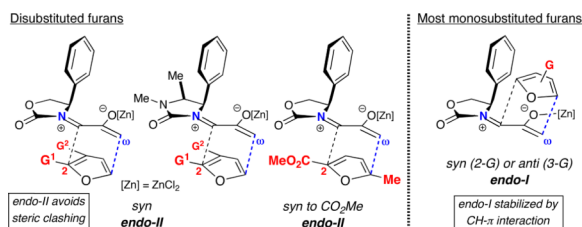
 Yunfei Du^a, Elizabeth H. Krenske^b, Jennifer E. Antoline^c, Andrew G. Lohse^c, K. N. Houk^d, and Richard P. Hsung^c
^aSchool of Pharmaceutical Science and Technology, Tianjin University, Tianjin, 300072, P. R. China

^bSchool of Chemistry, University of Melbourne, Victoria 3010, Australia, and Australian Research Council Centre of Excellence for Free Radical Chemistry and Biotechnology

^cDivision of Pharmaceutical Sciences and Department of Chemistry, University of Wisconsin at Madison, Madison, WI 53705

^dDepartment of Chemistry and Biochemistry, University of California, Los Angeles, CA 90095

Abstract



The regioselectivities and stereoselectivities of ZnCl₂-catalyzed (4+3) cycloadditions between chiral oxazolidinone-substituted oxyallyls and unsymmetrical disubstituted furans have been determined. The substitution pattern on the furan is found to provide a valuable tool for controlling the stereochemistry (*endo-I* or *endo-II*) of the 7-membered cycloadduct. While cycloadditions with monosubstituted furans usually favor *endo-I* products, from addition of the furan to the more crowded face of the oxyallyl, cycloadditions with 2,3- and 2,5-disubstituted furans instead favor the *endo-II* stereochemistry. Density functional theory calculations are performed to account for the selectivities. For monosubstituted furans, the crowded transition state leading to the *endo-I* cycloadduct is stabilized by an edge-to-face interaction between the furan and the oxazolidinone 4-Ph group, but this stabilization is overcome by steric clashing if the furan bears a 2-CO₂R group or is 2,3-disubstituted.

Correspondence to: Elizabeth H. Krenske; K. N. Houk; Richard P. Hsung.

ekrenske@unimelb.edu.au, houk@chem.ucla.edu, rhsung@wisc.edu.

Supporting Information

 NMR spectra and characterizations for all new compounds, X-ray Crystallographic Information Files and thermal ellipsoid plots, optimized geometries and energies, computed barriers at the B3LYP and B3LYP D3 levels for cycloadditions of **3b** and M06-2X barriers for **3c**. This material is available free of charge via the Internet at <http://pubs.acs.org>.

INTRODUCTION

Oxazolidinone-stabilized oxyallyls (**3**) are a fascinating class of reactive intermediates, generated by oxidation of allenamides (**1**).^{1,2} Several valuable synthetic routes to 7-membered carbocycles rely on (4+3) cycloadditions between oxyallyl intermediates and dienes,^{3,4} and we have found that the cycloadditions of oxyallyls **3** with monosubstituted furans (Schemes 1 and 2) display distinctive regioselectivities and stereoselectivities.^{5,6} These reactions may be performed either under thermal conditions or with catalysis by ZnCl₂. The regioselectivities are summarized in Scheme 1, which shows the achiral oxyallyl **3a**; cycloadditions of **3a** with 2-substituted furans (G = Me or CO₂Me) favor the “*syn*” regiochemistry, while reactions with 3-substituted furans favor “*anti*” regiochemistry. The same regioselectivities are obtained with the chiral oxyallyl **3b** (Scheme 2), but in this case the reactions also feature a novel mode of stereoinduction. Surprisingly, reactions of **3b** with most monosubstituted furans were found to favor the *endo-I* stereochemistry, which entails addition of the furan to the more crowded face of **3b**. Density functional theory calculations⁶ showed that the crowded transition state is favored because it contains a stabilizing edge-to-face aromatic interaction (CH– π) between furan and Ph. Of the monosubstituted furans studied, only those containing a 2-CO₂R group did not follow this behavior.

In order to explore the generality of these stereochemical and regiochemical control elements, we have examined the (4+3) cycloadditions of **3b** with more complex, unsymmetrical disubstituted furans. We report that these reactions often proceed with high levels of regio- and stereocontrol, even when the selectivities cannot be easily predicted from individual substituent effects. Complete control over stereoselectivity can be obtained through strategic choice of substituents.

RESULTS AND DISCUSSION

We investigated the (4+3) cycloadditions of oxyallyls **3** with a range of unsymmetrical disubstituted furans containing Me and CO₂Me substituents at different positions. The cycloadditions were performed under ZnCl₂-catalyzed conditions. Results are given in Table 1.

Our work commenced with the 2-CO₂Me,3-Me-substituted furan, **4**. Based on the selectivities previously observed with monosubstituted furans (Schemes 1 and 2), it is not possible to predict the major product for **4**; a 2-CO₂Me substituent favors *syn-II* but a 3-Me substituent favors *anti-I*. The cycloaddition of **3b** with **4** was found to give exclusively the *syn-II* cycloadduct, **8**, in 67% yield. The structure of **8** was assigned unambiguously by X-ray (Figure 1). The cycloaddition of **3b** with the 2-Me,3-CO₂Me-substituted furan **5** also gave exclusively a *syn-II* adduct (**9**). Confirmation of the structure of **9** was obtained following reduction/esterification, which afforded a rearranged derivative (**12**) whose X-ray structure was determined (Figure 1).⁷ The regioselectivities observed for both **4** and **5** match those previously obtained^{6b} with the achiral oxyallyl **3a**, which displayed *syn* selectivities of 95:5.

We next examined the 2-Me,3-Me-substituted furan, **6**. In order to deal with competing oxidation of this more electron-rich furan, we had to switch to the more reactive allenamide, **1c**,⁸ which contains Close's chiral imidazolidinone auxiliary.⁹ Previous experiments⁵ indicated that Close's imidazolidinone controls stereoselectivity in the same way as 4-Ph-oxazolidinone. Cycloaddition of **3c** with **6** afforded mainly the *syn-II* product, **10c**, but also gave two other cycloadducts: *syn-I* (**10a**) and *anti-I* (**10b**). X-ray structures were determined for the two minor products (Figure 1), while the major product was assigned unambiguously by NOESY and COSY (see Supporting Information).

In 2,3-disubstituted furans, the substituents have opposite regio-directing influences (Scheme 1) and the selectivities obtained with **4–6** indicate that it is the 2-substituent that dictates the outcome. In order to discern the relative directing power of Me and CO₂Me groups at the 2-position, we examined the reaction of **3b** with **7**. The only cycloadduct detected was **11**, where CO₂Me is *syn* to nitrogen. Its structure was confirmed by NOESY and COSY.

The regioselectivities and stereoselectivities observed here with disubstituted furans are quite distinct from those reported previously for monosubstituted furans.⁶ We performed density functional theory calculations to explore the selectivities. Transition states for ZnCl₂-catalyzed cycloadditions of the oxyallyls **3b** and **3c** with furans **4–7** were computed at the B3LYP/6-31G(d) level (with LANL2DZ on Zn), as we have previously done in our studies of related oxyallyl (4+3) cycloadditions. The transition states for the reaction of **3b** with **4** are representative and are shown in Figure 2. Regardless of the regiochemistry, the transition states each show the same sense of asynchronicity, with more advanced bonding at the unsubstituted terminus of the oxyallyl. The HOMO coefficient of the oxyallyl is larger at this terminus.

We previously found that B3LYP activation energies provide good predictions of regioselectivity and stereoselectivity for oxyallyl (4+3) cycloadditions. In order to provide a better treatment of dispersion energies in the cycloadditions of **4–7**, which are likely to vary significantly between stereoisomeric transition states *I* and *II*, we calculated the activation barriers from single-point energies at the M06-2X/6-311+G(d,p) level. Solvent effects were modeled by means of CPCM calculations. The M06-2X activation energies in the gas phase and in dichloromethane are given in Table 2.

The calculated values of ΔG^\ddagger in the gas phase and in solution predict a strong preference for the observed product (*syn-II*) for both furans **4** and **5**. The *syn-II*TS from **4** is favored by 2.9 kcal/mol in dichloromethane, and the *syn-II*TS from **5** is favored by 4.6 kcal/mol. Lower selectivity is predicted for furan **6**. Indeed, the cycloaddition of **6** with **3b** is calculated to favor the *anti-I*TS by 0.6 kcal/mol. However, the cycloaddition of the same furan with **3c**, which was studied experimentally, is correctly predicted to favor *syn-II*. The *syn-II*TS is preferred by 0.1–0.2 kcal/mol over *syn-I* and *anti-I*. Experimentally, a mixture of products was obtained containing the latter two isomers as minor products. The agreement between experiment and theory is not as good for **7**, where the calculations predict a 1.1 kcal/mol preference for *anti-I* in dichloromethane. The selectivity in the gas phase does correctly predict *syn-II*, however. Experimentally, the *syn-II* cycloadduct was obtained in 40% yield.

Activation energies were also computed with a second dispersion-inclusive functional, B3LYP-D3 (Supporting Information). The predicted selectivities mirror those from M06-2X. B3LYP alone also correctly predicts the major products for furans **4–6** (and from **7** in the gas phase), but fails to predict the presence of minor products in the cycloaddition involving **6**.

Our previous calculations showed that a 2-substituent on the furan favors *syn* regiochemistry because the shorter forming bond in the transition state is located at the less-hindered carbon (C-5) of the furan.⁶ When the 2-substituent is electron-withdrawing, this steric effect is reinforced by a strong oxyallyl–furan interaction energy, related to the large furan LUMO coefficient at C-5. For 3-substituted furans, by contrast, the *anti* regiochemistry is favored because its transition state avoids steric clashing between the 3-substituent and the oxazolidinone.

The *syn* selectivities obtained experimentally from furans **4–7** (Table 1) indicate that the regio-directing influence of a 2-substituent outweighs that of a 3-substituent, regardless of whether the substituent is Me or CO₂Me. A 2-CO₂Me group exerts a stronger regio-directing effect than a 2-Me group (cf. **7**), because the oxyallyl–furan interaction in the TS is stronger when CO₂Me is *syn* to nitrogen.

The stereoselectivities observed with furans **4–7** cannot be predicted from those of the corresponding monosubstituted furans. Most monosubstituted furans favor diastereomer *I*, due to the stabilizing edge-to-face aryl–aryl interaction in the crowded (*I*) transition state (Scheme 2).^{6a,c} Only for 2-CO₂Me-furan was *II* favored; in that case, the (*syn*)-*ITS* is destabilized by electrostatic repulsion between the CO₂Me group and the Ph π -cloud.

A similar type of repulsive electrostatic effect influences the stereoselectivities for **4** and **7**, favoring *II*. More generally, however, the stereoselectivities for all three 2,3-disubstituted furans (**4–6**) are dictated by the furan 3-substituent. This group eliminates the possibility of an edge-to-face CH– π interaction in the crowded *syn*-*ITS*, and replaces it with a repulsive electrostatic interaction (3-CO₂Me) or a weaker CH– π interaction (3-Me). The result is a preference for *II*. Only for **6**, where no CO₂Me group is present, are isomers of *I* found as minor products.

CONCLUSION

The investigations detailed herein provide a valuable new approach to controlling the stereoselectivities of (4+3) cycloadditions. The different classes of substituent effects operating for monosubstituted and disubstituted furans are outlined in Scheme 3, and can be summarized as follows: cycloaddition of oxyallyl **3b** or **3c** with a 2-substituted furan (including a disubstituted furan) favors the *syn-I* cycloadduct, unless (a) the 2-substituent is CO₂R or (b) there is also a substituent present at furan C-3. In the latter two cases, *syn-II* is preferred instead. These principles enable cycloadditions of oxyallyls **3** with complex furans to be achieved with high levels of regioselectivity and stereoselectivity.

EXPERIMENTAL SECTION

General Procedure for Allenamide (**4** + **3**) Cycloadditions

To a solution of a respective allenamide in CH₂Cl₂ (0.1 M) was added 3–9 equiv of the appropriate furan and 4 Å powdered molecular sieves [0.5 g]. The reaction solution was cooled to –78 °C, and 2.0 equiv of ZnCl₂ (1.0 M in Et₂O) was added. 4.0–6.0 equiv of dimethyldioxirane [DMDO] in acetone was then added as a chilled solution [at –78 °C] via a syringe pump over 3–4 h. The syringe pump was cooled using dry ice during the entire addition time. After the addition, the reaction mixture was stirred for an additional 14 h before it was quenched with sat aq NaHCO₃, filtered through Celite™, concentrated *in vacuo*, and extracted with CH₂Cl₂ [4 × 20 mL]. The combined organic layers were dried over Na₂SO₄ and concentrated *in vacuo*. The crude residue was purified via silica gel column chromatography [gradient eluent: 10% to 75% ethyl acetate in hexane].

8: Reaction Scale: 0.50 mmol of allenamide **1b**; Yield: 67%; mass: 119.6 mg. R_f = 0.13 (50% EtOAc in hexane); [α]_D²³ –169.6° [c 4.6, CH₂Cl₂]; white solid; mp = 119–120 °C; ¹H NMR (400 MHz, CDCl₃) δ 2.04 (s, 3H), 2.54 (d, 1H, *J* = 16.0 Hz), 2.83 (dd, 1H, *J* = 5.4, 16.0 Hz), 3.29 (s, 3H), 3.91 (s, 1H), 4.20 (t, 1H, *J* = 9.0 Hz), 4.62 (t, 1H, *J* = 9.0 Hz), 4.79 (t, 1H, *J* = 9.0 Hz), 4.90 (dt, 1H, *J* = 5.2, 1.6 Hz), 7.00 (d, 1H, *J* = 1.6 Hz), 7.31–7.45 (m, 5H); ¹³C NMR (100 MHz, CDCl₃) δ 15.3, 44.3, 52.6, 65.9, 68.5, 70.5, 76.8, 88.3, 128.7, 129.3, 129.7, 130.2, 136.6, 142.9, 158.5, 166.9, 200.9; IR (thin film) cm^{–1} 3280w, 2911w,

1766s, 1437w; mass spectrum (APCI): m/e (% relative intensity) 358.1 (100) (M + H)⁺; HRMS (MALDI-TOF): m/e calcd for C₁₉H₁₉NO₆Na⁺ (M+Na⁺) 380.1105, found 380.1097.

9: Reaction Scale: 1.00 mmol of allenamide **1b**; Yield: 60%; mass: 214.2 mg. R_f = 0.25 (50% EtOAc in hexane); [α]_D²³ -74.5 ° [c 4.0, CH₂Cl₂]; ¹H NMR (500 MHz, CDCl₃) δ 1.30 (s, 3H), 2.60 (d, 1H, J = 17.5 Hz), 2.88 (dd, 1H, J = 6.0, 17.5 Hz), 3.45 (s, 1H), 3.80 (s, 3H), 4.36 (t, 1H, J = 9.0 Hz), 4.71 (t, 1H, J = 9.0 Hz), 4.83 (t, 1H, J = 9.0 Hz), 4.99 (dd, 1H, J = 6.0, 2.0 Hz), 7.08 (d, 1H, J = 0.25 Hz), 7.48 – 7.52 (m, 5H); ¹³C NMR (125 MHz, CDCl₃) δ 15.4, 44.3, 52.6, 66.0, 68.6, 70.6, 76.9, 88.4, 126.4, 128.8, 129.4, 129.8, 130.3, 143.0, 158.6, 167.0, 201.0; IR (thin film) cm⁻¹ 2954s, 2930s, 1764s, 1726s; mass spectrum (APCI): m/e (% relative intensity) 358.2 (100) (M + H)⁺; HRMS (MALDI-TOF): m/e calcd for C₁₉H₁₉NO₆Na⁺ (M+Na⁺) 380.1105, found 380.1095.

10a: Reaction Scale: 0.44 mmol of allenamide **1c**; Yield: 9%; mass: 13.5 mg. R_f = 0.22 (50% EtOAc in hexane); [α]_D²³ +14.9 ° [c 0.75, CH₂Cl₂]; mp = 162 – 163 °C; ¹H NMR (400 MHz, CDCl₃) δ 0.79 (d, 1H, J = 6.8 Hz), 1.46 (s, 3H), 1.81 (s, 3H), 2.49 (d, 1H, J = 17.8 Hz), 2.60 (dd, 1H, J = 5.8, 17.8 Hz), 2.69 (s, 3H), 3.29 (s, 1H), 3.82 (dq, 1H, J = 6.8, 9.2 Hz), 4.70 (d, 1H, J = 9.2 Hz), 4.75 (d, 1H, J = 5.8 Hz), 5.91 (s, 1H), 7.13 (br, 1H), 7.32 (br, 4H); ¹³C NMR (100 MHz, CDCl₃) δ 14.0, 15.5, 21.4, 29.3, 43.8, 56.6, 65.2, 69.3, 75.9, 86.8, 128.5, 128.8, 128.9, 129.5, 135.3, 144.8, 159.3, 200.9; IR (thin film) cm⁻¹ 2929m, 1725s, 1687s, 1432m, 1263m, 1161m, 736m, 694s; mass spectrum (APCI): m/e (% relative intensity) 341.2 (60) (M + H)⁺; HRMS (MALDI-TOF): m/e calcd for C₂₀H₂₄N₂O₃Na⁺ (M + Na⁺) 363.1679, found 363.1680.

10b: Reaction Scale: 0.44 mmol of allenamide **1c**; Yield: 21%; mass: 31.4 mg. R_f = 0.17 (50% EtOAc in hexane); [α]_D²³ -184.3 ° [c 0.79, CH₂Cl₂]; white solid; mp = 194 – 195 °C; ¹H NMR (400 MHz, CDCl₃) δ 0.71 (d, 1H, J = 6.8 Hz), 1.34 (s, 3H), 1.59 (s, 3H), 2.44 (d, 1H, J = 15.6 Hz), 2.57 (d, 1H, J = 15.6 Hz), 2.73 (s, 3H), 3.96 (dq, 1H, J = 6.8, 8.8 Hz), 4.46 (d, 1H, J = 8.8 Hz), 4.49 (d, 1H, 4.2 Hz), 4.66 (s, 1H), 5.10 (d, 1H, J = 4.2 Hz), 7.03 (br, 1H), 7.31-7.33 (m, 1H); ¹³C NMR (100 MHz, CDCl₃) δ 12.1, 15.3, 21.6, 29.3, 50.8, 57.2, 59.7, 64.5, 79.2, 85.9, 125.6, 127.4, 128.4, 129.2, 138.8, 146.3, 162.6, 203.8; IR (thin film) cm⁻¹ 2941m, 1728s, 1686s, 1431m, 1255m, 1196s, 1025m, 855s, 735s, 700s; mass spectrum (APCI): m/e (% relative intensity) 339.2 (45) (M - H)⁻; HRMS (MALDI-TOF): m/e calcd for C₂₀H₂₄N₂O₃Na⁺ (M+Na⁺) 363.1679, found 363.1678.

10c: Reaction Scale: 0.44 mmol of allenamide **1c**; Yield: 31%; mass: 46.4 mg. R_f = 0.23 (50% EtOAc in hexane); [α]_D²³ -105.7 ° [c 0.83, CH₂Cl₂]; colorless oil; ¹H NMR (400 MHz, CDCl₃) δ 0.85 (d, 1H, J = 6.8 Hz), 1.13 (s, 3H), 1.89 (s, 3H), 2.47 (d, 1H, J = 17.2 Hz), 2.71 (dd, 1H, J = 5.8, 17.2 Hz), 2.79 (s, 3H), 3.43 (s, 1H), 3.92 (dq, 1H, J = 6.8, 9.2 Hz), 4.61 (d, 1H, J = 9.2 Hz), 4.74 (d, 1H, J = 5.8 Hz), 5.86 (s, 1H), 7.27-7.34 (m, 5H); ¹³C NMR (100 MHz, CDCl₃) δ 14.4, 15.1, 21.4, 29.1, 44.7, 56.3, 68.1, 74.9, 75.9, 87.7, 121.1, 128.5, 128.8, 129.5, 137.0, 146.9, 161.7, 204.2; IR (thin film) cm⁻¹ 2933m, 1703s, 1431, 1400s, 1262m, 1159m, 762m; mass spectrum (APCI): m/e (% relative intensity) 341.2 (60) (M + H)⁺; HRMS (MALDI-TOF): m/e calcd for C₂₀H₂₄N₂O₃Na⁺ (M+Na⁺) 363.1679, found 363.1674.

11: Reaction Scale: 0.35 mmol of allenamide **1b**; Yield: 40%; mass: 50.0 mg. R_f = 0.22 (50% EtOAc in hexane); [α]_D²³ -31.4 ° [c 6.4, CH₂Cl₂]; ¹H NMR (500 MHz, CDCl₃) δ 1.43 (s, 3H), 2.59 (d, 1H, J = 16.0 Hz), 2.68 (dd, 1H, J = 5.2, 16.0 Hz), 3.65 (s, 3H), 3.93 (s, 1H), 4.18 (t, 1H, J = 9.0 Hz), 4.65 (t, 1H, J = 9.0 Hz), 4.82 (t, 1H, J = 9.0 Hz), 6.07 (d, 1H, J = 6.0 Hz), 6.66 (d, 1H, J = 6.0 Hz), 7.28 – 7.41 (m, 5H); ¹³C NMR (100 MHz, CDCl₃) δ 23.2, 51.3, 64.4, 67.2, 70.5, 72.8, 86.1, 89.4, 126.4, 128.4, 129.9, 133.4, 135.6, 136.5, 158.1, 167.5, 199.8; IR (thin film) cm⁻¹ 3520w, 2957w, 2927w, 1759s, 1726s; mass spectrum

(APCI): m/e (% relative intensity) 358.2 (35) ($M + H$)⁺; HRMS (MALDI-TOF): m/e calcd for $C_{19}H_{19}NO_6Na^+$ ($M+Na^+$) 380.1105, found 380.1090.

Synthesis of Ester 12 from Cycloadduct 9

To a solution of cycloadduct **9** (53.6 mg, 0.150 mmol) in anhyd MeOH (5 mL) was added $NaBH_4$ (34.2 mg, 0.904 mol) portion-wise within 1 h at 0 °C. The reaction mixture was further stirred at room temperature for 6 h until the consumption of the starting material. Sat aq NaCl (10 mL) was added to quench the reaction. After removal of the volatile solvent under reduced pressure, the aqueous residue was extracted with CH_2Cl_2 (3×10 mL). The combined organic layer was dried over Na_2SO_4 and concentrated *in vacuo*, and the crude residue was directly used for the next step.

The above crude residue was taken up in CH_2Cl_2 (5 mL), and to this solution were added DMAP (1.1 mg, 0.009 mmol) and Et_3N (0.06 mL, 0.431 mmol) with vigorous stirring under ice-water cooling bath. After which, 2,4,6-trichlorobenzoyl chloride (0.07 mL, 0.450 mmol) was then added in one portion. The reaction mixture was stirred at rt for 30 h, and was then quenched with cold H_2O (10 mL), and extracted with CH_2Cl_2 [4×20 mL]. The combined organic layers were dried over Na_2SO_4 and concentrated *in vacuo*. The crude residue was purified via silica gel column chromatography [gradient eluent: 10% to 30% EtOAc in hexane] to give the pure ester **12** (35.3 mg, 0.062 mmol, 42% over two steps) as a white solid.

12: R_f = 0.21 (30% EtOAc in hexane); $[\alpha]_D^{23} + 29.9^\circ$ [c 1.05, CH_2Cl_2]; white solid; mp = 176 – 177 °C; 1H NMR (400 MHz, $CDCl_3$) δ 1.66 (s, 3H), 2.01 – 2.14 (m, 2H), 2.29 (dt, 1H, J = 8.4, 12.0 Hz), 2.56 (ddd, 1H, J = 2.4, 8.8, 12.0 Hz), 2.79 (dd, 1H, J = 8.8, 11.6 Hz), 3.35 (s, 3H), 3.37 (d, 1H, J = 7.2 Hz), 4.35 (br, 1H); 4.39 (t, 1H, J = 6.4 Hz); 4.84 – 4.89 (m, 2H); 4.95 (q, 1H, J = 7.2 Hz), 7.54 (d, 1H, J = 1.4 Hz), 7.52 (d, 1H, J = 1.4 Hz), 7.35 – 7.41 (m, 3H), 7.31 (s, 2H); ^{13}C NMR (100 MHz, $CDCl_3$) δ 26.8, 31.2, 33.7, 51.8, 52.3, 60.9, 63.7, 64.4, 72.0, 74.1, 82.2, 128.3, 129.1, 129.2, 131.7, 132.8, 135.2, 136.7, 159.3, 163.6, 169.8 (one carbon peak was missing due to overlapping); IR (thin film) cm^{-1} 2955m, 1755s, 1579m, 1373m, 1265s, 1209m, 1117m, 734m; mass spectrum (APCI): m/e (% relative intensity) 574.0 (7) ($M + 6 + H$)⁺; 572.1 (33) ($M + 4 + H$)⁺; 569.2 (30) ($M + 2$)⁺, 568.1 (96) ($M + H$)⁺; 567.1 (90) (M)⁺, 419.4 (9), 344.2 (22), 329.0 (85), 328.1 (21), 327.0 (100); HRMS (MALDI-TOF): m/e calcd for $C_{26}H_{24}Cl_3NO_7Na^+$ ($M+Na^+$) 590.0516, found 590.0511.

THEORETICAL CALCULATIONS

Density functional theory calculations were performed in Gaussian 09.¹⁰ Geometries were optimized in the gas phase using the B3LYP¹¹ functional, with a mixed basis set consisting of LANL2DZ on Zn and 6-31G(d) on all other atoms. The lowest-energy conformer of each species was identified through conformational searching. The B3LYP vibrational frequencies were used to characterize species as minima or transition states, and to obtain scaled¹² zero-point energies and thermal contributions to enthalpy and entropy. Single-point energies were then computed at the M06-2X/6-311+G(d,p) level,¹³ and used in conjunction with the B3LYP thermochemical corrections to obtain gas-phase activation enthalpies and free energies. Free energies of activation in dichloromethane were calculated by incorporating CPCM¹⁴ solvation energies computed at the M06-2X/6-31G(d)–LANL2DZ level (UAKS radii). A standard state of 1 mol/L was used. Activation energies were also computed from single-point energy calculations at the B3LYP-D3¹⁵ level, with zero-damping. The activation energies predicted by B3LYP and B3LYP-D3 for cycloadditions involving **3b** are provided in the Supporting Information, along with M06-2X activation energies for cycloadditions of **3c** with **4–7**.

Supplementary Material

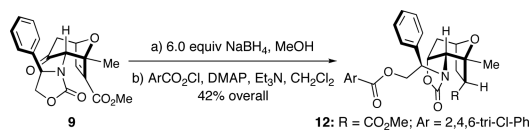
Refer to Web version on PubMed Central for supplementary material.

Acknowledgments

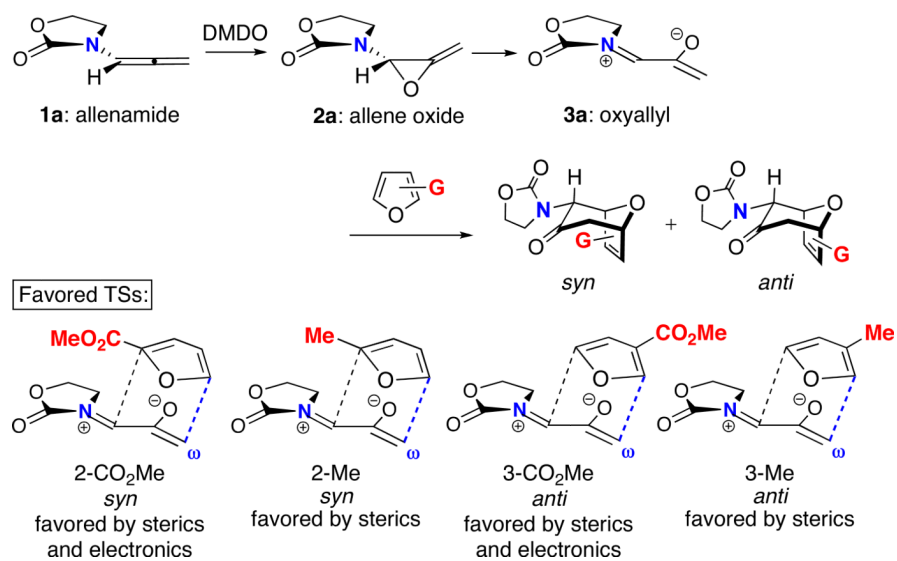
We thank the NIH and Australian Research Council for generous financial support (GM-36700 to K.N.H., GM-66055 to R.P.H., and DP0985623 to E.H.K.), and the National Computational Infrastructure National Facility (Australia) and University of Melbourne for computer resources. E.H.K. also thanks the ARC Centre of Excellence for Free Radical Chemistry and Biotechnology for financial support. We thank Dr. Vic Young and Mr. Gregory T. Rohde of The University of Minnesota for X-ray crystallography.

REFERENCES

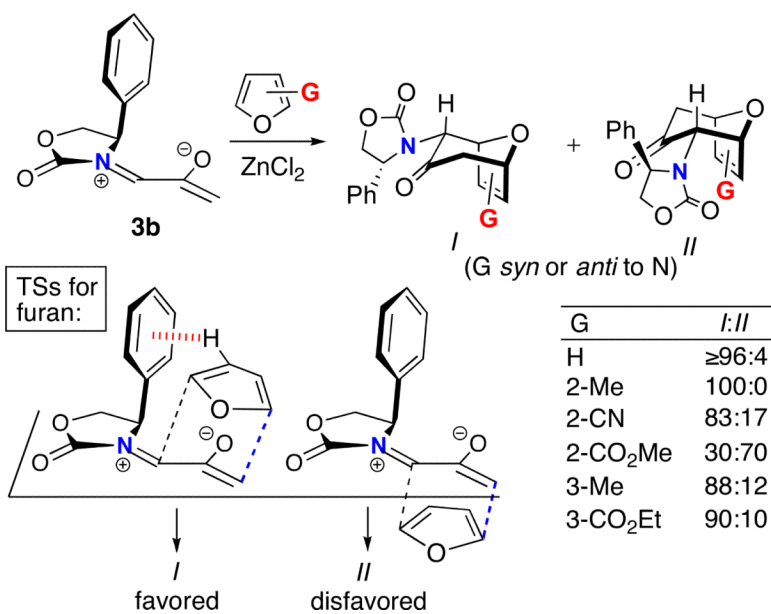
1. For a key review on allenamide chemistry, see: Wei L-L, Xiong H, Hsung RP. *Acc. Chem. Res.* 2003; 36:773–782. [PubMed: 14567711]
2. For recent reviews on heteroatom-substituted oxyallyl intermediates, see: Lohse AG, Hsung RP. *Chem. Eur. J.* 2011; 17:3812–3822. [PubMed: 21384451] Harmata M. *Chem. Commun.* 2010; 46:8904–8922. Harmata M. *Recent Res. Devel. Org. Chem.* 1997; 1:523–535.
3. For general reviews on (4+3) cycloadditions, see: Harmata M. *Chem. Commun.* 2010; 46:8886–8903. Harmata M. *Adv. Synth. Catal.* 2006; 348:2297–2306. Battiste MA, Pelphrey PM, Wright DL. *Chem. Eur. J.* 2006; 12:3438–3447. [PubMed: 16402402] Hartung IV, Hoffmann HMR. *Angew. Chem. Int. Ed.* 2004; 43:1934–1949. Rigby JH, Pigge FC. *Org. React.* 2004:351–478. Harmata M, Rashatasakhon P. *Tetrahedron.* 2003; 59:2371–2395. Harmata M. *Acc. Chem. Res.* 2001; 34:595–605. [PubMed: 11456477] Davies HML. Harmata M. *Advances in Cycloaddition.* 1999; 5:119–164. JAIStamford, CT West FG. Lautens M. *Advances in Cycloaddition.* 1997; 4:1–40. JAIGreenwich, CT Harmata M. *Tetrahedron.* 1997; 53:6235–6280. Katritzky AR, Dennis N. *Chem. Rev.* 1989; 89:827–861.
4. For (4+3) cycloadditions of donor-substituted oxyallyls, including regioselective examples, see: Föhlisch B, Krimmer D, Gehrlach E, Kaeshammer D. *Chem. Ber.* 1988; 121:1585–1594. Murray DH, Albizati KF. *Tetrahedron Lett.* 1990; 31:4109–4112. Walters MA, Arcand HR, Lawrie DJ. *Tetrahedron Lett.* 1995; 36:23–26. Lee JC, Jin S, Cha JK. *J. Org. Chem.* 1998; 63:2804–2805. Harmata M, Rashatasakhon P. *Synlett.* 2000:1419–1422. Beck H, Stark CBW, Hoffmann HMR. *Org. Lett.* 2000; 2:883–886. [PubMed: 10768177] Myers AG, Barbay JK. *Org. Lett.* 2001; 3:425–428. [PubMed: 11428030] Harmata M, Ghosh SK, Hong X, Wacharasindhu S, Kirchoefer P. *J. Am. Chem. Soc.* 2003; 125:2058–2059. [PubMed: 12590528] MaGee DI, Godineau E, Thornton PD, Walters MA, Sponholtz DJ. *Eur. J. Org. Chem.* 2006:3667–3680. Chung WK, Lam SK, Lo B, Liu LL, Wong W-T, Chiu P. *J. Am. Chem. Soc.* 2009; 131:4556–4557. [PubMed: 19281161] Lo B, Chiu P. *Org. Lett.* 2011; 13:864–867. [PubMed: 21275427] Liu LL, Chiu P. *Chem. Commun.* 2011; 47:3416–3417.
5. For our contributions to the field of (4+3) cycloadditions, see: Xiong H, Hsung RP, Berry CR, Rameshkumar C. *J. Am. Chem. Soc.* 2001; 123:7174–7175. [PubMed: 11459504] Xiong H, Hsung RP, Shen L, Hahn JM. *Tetrahedron Lett.* 2002; 43:4449–4453. Rameshkumar C, Xiong H, Tracey MR, Berry CR, Yao LJ, Hsung RP. *J. Org. Chem.* 2002; 67:1339–1345. [PubMed: 11846684] Xiong H, Huang J, Ghosh SK, Hsung RP. *J. Am. Chem. Soc.* 2003; 125:12694–12695. [PubMed: 14558802] Rameshkumar C, Hsung RP. *Angew. Chem. Int. Ed.* 2004; 43:615–618. Huang J, Hsung RP. *J. Am. Chem. Soc.* 2005; 127:50–51. [PubMed: 15631443] Antoline JE, Hsung RP, Huang J, Song Z, Li G. *Org. Lett.* 2007; 9:1275–1278. [PubMed: 17335226] Antoline JE, Hsung RP. *Synlett.* 2008:739–744. Lohse AG, Hsung RP, Leider MD, Ghosh SK. *J. Org. Chem.* 2011; 76:3246–3257. [PubMed: 21449577]
6. a Krenske EH, Houk KN, Lohse AG, Antoline JE, Hsung RP. *Chem. Sci.* 2010; 1:387–392. [PubMed: 21572919] b Lohse AG, Krenske EH, Antoline JE, Houk KN, Hsung RP. *Org. Lett.* 2010; 12:5506–5509. [PubMed: 21049917] c Antoline JE, Krenske EH, Lohse AG, Houk KN, Hsung RP. *J. Am. Chem. Soc.* 2011; 133:14443–14451. [PubMed: 21851070]
7. During the synthesis of ester **12** from cycloadduct **9**, an acyl transfer occurred during the esterification step.



8. a Wei L-L, Hsung RP, Xiong H, Mulder JA, Nkansah NT. *Org. Lett.* 1999; 1:2145–2148. b Berry CR, Hsung RP, Antoline JE, Petersen ME, Challeppan R, Nielson JA. *J. Org. Chem.* 2005; 70:4038–4042. [PubMed: 15876094]
9. a Close WJ. *J. Org. Chem.* 1950; 15:1131–1134. b Roder H, Helmchen G, Peters E-M, Peters K, von Schnering H-G. *Angew. Chem.* 1984; 96:895–896.
10. Frisch, MJ.; Trucks, GW.; Schlegel, HB.; Scuseria, GE.; Robb, MA.; Cheeseman, JR.; Scalmani, G.; Barone, V.; Mennucci, B.; Petersson, GA.; Nakatsuji, H.; Caricato, M.; Li, X.; Hratchian, HP.; Izmaylov, AF.; Bloino, J.; Zheng, G.; Sonnenberg, JL.; Hada, M.; Ehara, M.; Toyota, K.; Fukuda, R.; Hasegawa, J.; Ishida, M.; Nakajima, T.; Honda, Y.; Kitao, O.; Nakai, H.; Vreven, T.; Montgomery, JA., Jr.; Peralta, JE.; Ogliaro, F.; Bearpark, M.; Heyd, JJ.; Brothers, E.; Kudin, KN.; Staroverov, VN.; Kobayashi, R.; Normand, J.; Raghavachari, K.; Rendell, A.; Burant, JC.; Iyengar, SS.; Tomasi, J.; Cossi, M.; Rega, N.; Millam, JM.; Klene, M.; Knox, JE.; Cross, JB.; Bakken, V.; Adamo, C.; Jaramillo, J.; Gomperts, R.; Stratmann, RE.; Yazyev, O.; Austin, AJ.; Cammi, R.; Pomelli, C.; Ochterski, JW.; Martin, RL.; Morokuma, K.; Zakrzewski, VG.; Voth, GA.; Salvador, P.; Dannenberg, JJ.; Dapprich, S.; Daniels, AD.; Farkas, Ö.; Foresman, JB.; Ortiz, JV.; Cioslowski, J.; Fox, DJ. *Gaussian 09*, Revision A.02. Gaussian, Inc.; Wallingford CT: 2009.
11. a Lee C, Yang W, Parr RG. *Phys. Rev. B.* 1988; 37:785–789. b Becke AD. *J. Chem. Phys.* 1993; 98:1372–1377. c Becke AD. *J. Chem. Phys.* 1993; 98:5648–5652.
12. Merrick JP, Moran D, Radom L. *J. Phys. Chem. A.* 2007; 111:11683–11700. [PubMed: 17948971]
13. a Zhao Y, Truhlar DG. *Theor. Chem. Acc.* 2008; 120:215–241. b Zhao Y, Truhlar DG. *Acc. Chem. Res.* 2008; 41:157–167. [PubMed: 18186612]
14. a Barone V, Cossi M. *J. Phys. Chem. A.* 1998; 102:1995–2001. b Cossi M, Rega N, Scalmani G, Barone V. *J. Comput. Chem.* 2003; 24:669–681. [PubMed: 12666158]
15. Grimme S, Antony J, Ehrlich S, Krieg H. *J. Chem. Phys.* 2010; 132:154104. [PubMed: 20423165]



Scheme 1. Regioselectivities of (4+3) Cycloadditions of Achiral Oxyallyl **3a** with Monosubstituted Furans.^{6b}



Scheme 2.
Stereoselectivities of (4+3) Cycloadditions of Chiral Oxyallyl **3b** with Monosubstituted Furans.^{6a,c}

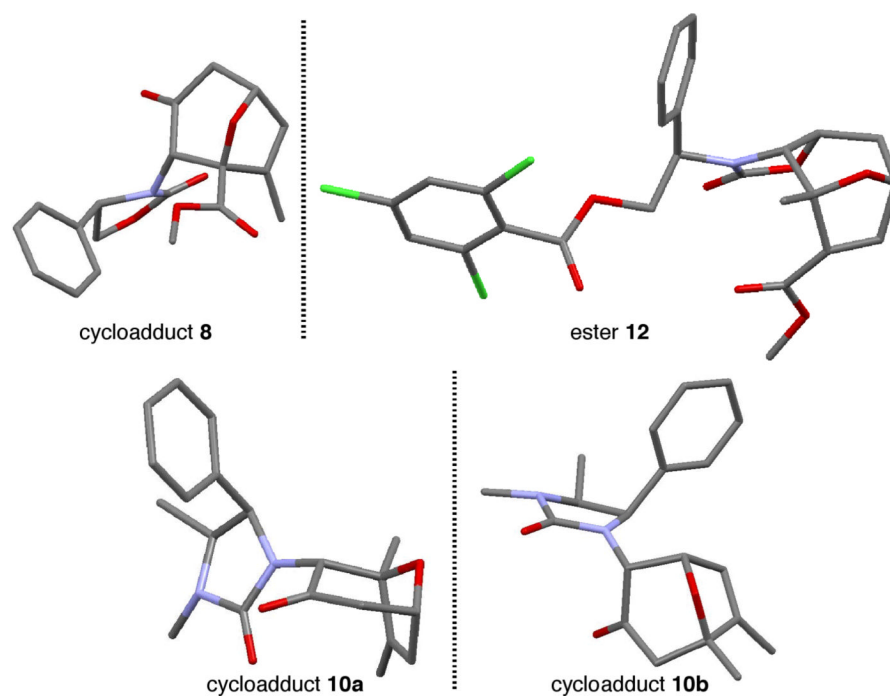


Figure 1. X-Ray structures of cycloadduct **8**, ester **12** (derived from **9**), and cycloadducts **10a** and **10b**.

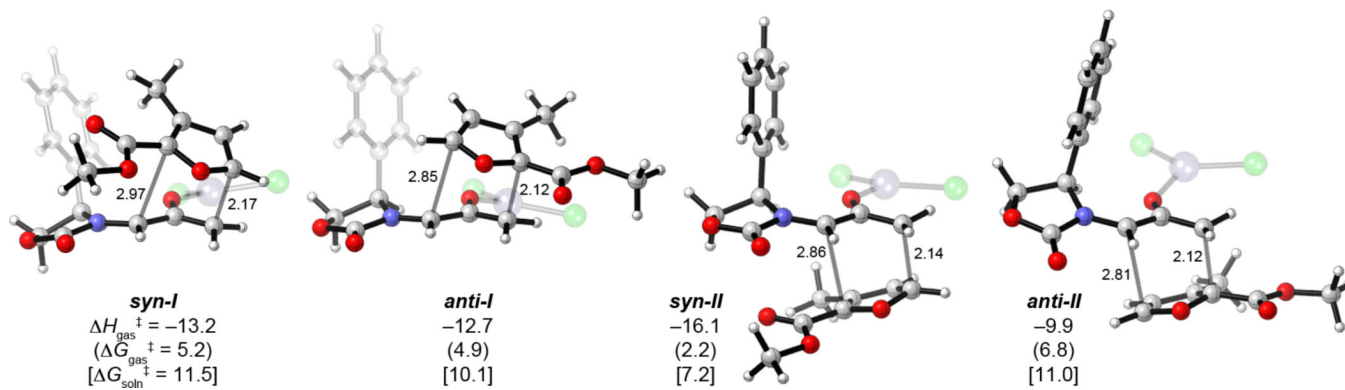
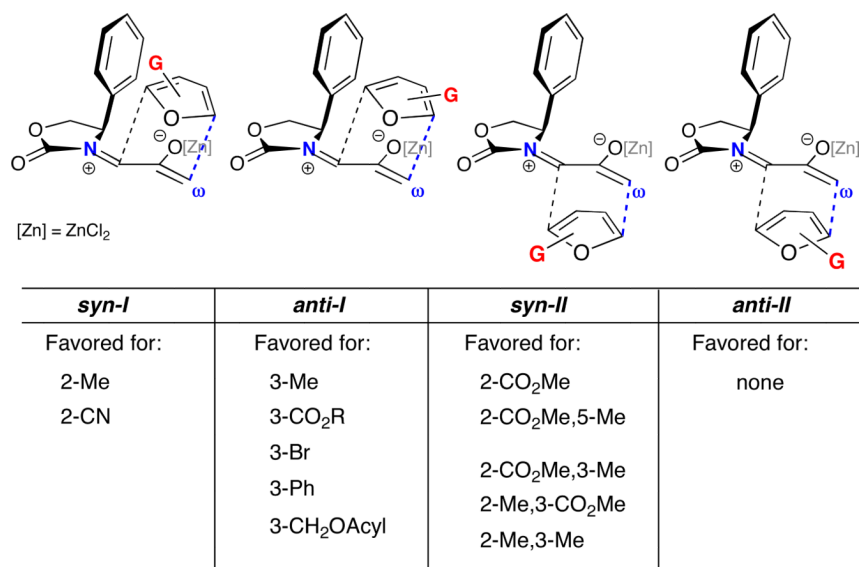
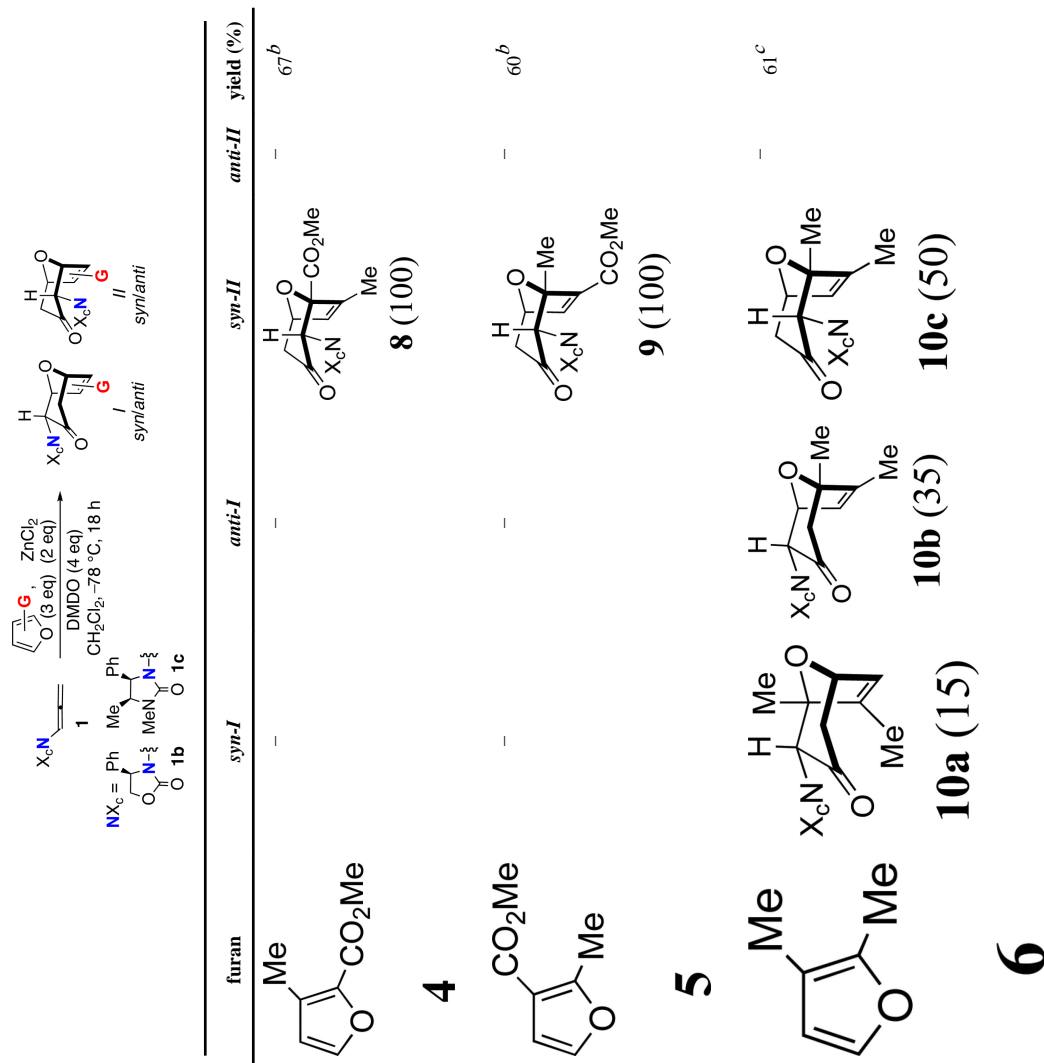


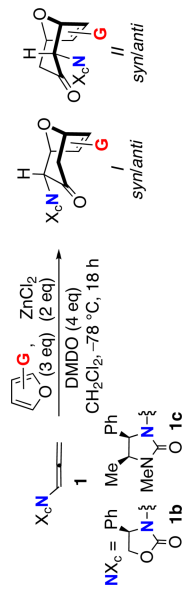
Figure 2. Transition structures for ZnCl_2 -catalyzed cycloadditions of oxyallyl **3b** with furan **4**, optimized with B3LYP. Below each structure are given the activation energies obtained from M06-2X single-point calculations. Distances in Å, ΔH^{\ddagger} and ΔG^{\ddagger} in kcal/mol.



Scheme 3.
Summary of Substituent-Controlled Regioselectivity and Stereoselectivity in (4+3)
Cycloadditions of Oxyallyl **3b** with Furans

Table 1

(4+3) Cycloadditions of Oxyallyls with Disubstituted Furan.^a



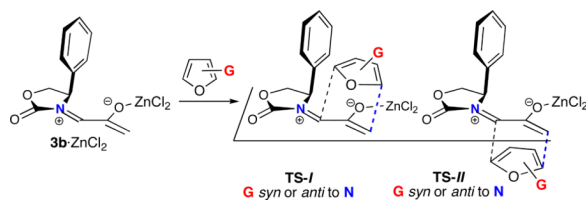
furan	syn- <i>I</i>	anti- <i>I</i>	syn- <i>II</i>	anti- <i>II</i>	yield (%)
 7	–	–	 11 (100)	–	40 ^b

^a Isolated yields are quoted. Isomer ratios are given in parentheses and were determined by ^1H and/or ^{13}C -NMR.

^b From reaction with allenamide **1b**.

^c From reaction with allenamide **1c**.

Table 2

Calculated Activation Energies for ZnCl₂-Catalyzed Cycloadditions of **3b** with Disubstituted Furans.^a

Reactants	ΔH^\ddagger (ΔG^\ddagger) [$\Delta G_{\text{soln}}^\ddagger$]			
	<i>syn-I</i>	<i>anti-I</i>	<i>syn-II</i>	<i>anti-II</i>
4 + 3b -ZnCl ₂	-13.2 (5.2) [11.5]	-12.7 (4.9) [10.1]	-16.1 (2.2) [7.2]	-9.9 (6.8) [11.0]
5 + 3b -ZnCl ₂	-13.2 (4.3) [12.5]	-15.5 (3.6) [11.9]	-14.6 (2.6) [7.3]	-13.0 (5.6) [14.1]
6 + 3b -ZnCl ₂	-12.8 (3.9) [8.4]	-15.0 (2.3) [7.4]	-12.1 (3.6) [8.0]	-12.4 (3.9) [8.0]
6 + 3c -ZnCl ₂	-7.0 (9.7) [14.3]	-8.3 (9.0) [14.4]	-6.1 (9.6) [14.2]	-6.0 (10.4) [14.9]
7 + 3b -ZnCl ₂	-9.6 (8.4) [16.1]	-11.5 (4.8) [9.9]	-14.4 (3.8) [11.0]	-8.3 (7.0) [11.4]

^aM06-2X/6-311+G(d,p)//B3LYP/6-31G(d)-LANL2DZ. Solution-phase data incorporate CPCM solvation energies in CH₂Cl₂, computed at the M06-2X/6-31G(d)-LANL2DZ level. ΔH^\ddagger and ΔG^\ddagger in kcal/mol at 298.15 K.